

The effects of the QCD critical point on the spectra and flow coefficients of hadrons

Sushant K. Singh^{1,2,*} and Jan-e Alam^{1,2}

¹Variable Energy Cyclotron Centre, 1/AF, Bidhan Nagar, Kolkata, India

²HBNI, Training School Complex, Anushakti Nagar, Mumbai 400085, India

(Dated: May 31, 2022)

The space-time evolution of the hot and dense fireball of quarks and gluons produced in ultra-relativistic heavy-ion collisions at non-zero baryonic chemical potential and temperature has been studied by using relativistic viscous causal hydrodynamics. For this purpose a numerical code has been developed to solve the relativistic viscous causal hydrodynamics in (3+1)-dimensions with the inclusion of QCD critical point (CP) through the equation of state and scaling behaviour of the transport coefficients. We have evaluated the transverse momentum spectra, directed and elliptic flow coefficients of pions and protons to comprehend the effect of CP on these observables by using this code. It is found that the integration over the entire space-time history of the fireball largely obliterates the effects of CP on the spectra and flow coefficients.

PACS numbers:

Keywords: QGP, Critical Point, Hydrodynamics.

I. INTRODUCTION

Calculations based on lattice QCD (Quantum Chromodynamics) and effective field theoretical models at non-zero temperature (T) and baryonic chemical potential (μ_B) affirm a complex phase diagram [1–6]. It is established by lattice QCD calculations that at high T and low μ_B ($\rightarrow 0$) the quark-hadron transition is a crossover. However, the transition may be first order in nature [5, 7] at low T and high μ_B . Therefore, it is expected that between the crossover and the first order transition there may exist a point in the $\mu_B - T$ plane, called the Critical End Point or simply Critical Point (CP) where the first order transition ends and the cross over begins [8]. The location of the CP is not yet precisely known from the lattice QCD based calculations [9] due to well-known sign problem for spin 1/2 particle (quark) [10] at non-zero μ_B .

However, there are several calculations based on effective field theoretic models at non-zero baryon density [11–14] predicting diverse locations for the CP in the $\mu_B - T$ plane [15]. The coordinates of the CP, (μ_{Bc}, T_c) , depend on the values of the parameters of the model. In the present work we take, $(\mu_{Bc}, T_c) = (350 \text{ MeV}, 143.2 \text{ MeV})$ as a representing point for CP in the QCD phase diagram. It is expected that the physical behaviour of the system reflected through various observables will not depend on a particular choice of (μ_{Bc}, T_c) .

It is generally accepted that the quark gluon plasma (QGP) system formed with small μ_B and high T in nuclear collisions at top Relativistic Heavy Ion Collider (RHIC) and Large Hadron Collider (LHC) energies revert to hadronic phase via cross over transition. The ongoing Beam Energy Scan - II program at RHIC, the upcoming Compressed Baryonic Matter (CBM) and the Nuclotron based Ion Collider fAcility (NICA) experiments are projected to produce QGP at high μ_B and lower T which revert to hadronic phase through a first order phase transition. The QCD matter at different values T and μ_B can be produced in nuclear collisions by regulating the center of mass energy per nucleon ($\sqrt{s_{NN}}$) of the colliding nuclei and scanning through different rapidities at a given colliding energy. Therefore, the colliding energy and the rapidity (y) bin should judiciously be chosen to approach the critical point at (μ_{Bc}, T_c) .

Several signatures of the CP has been proposed in the literature. One of the early work [16] predicts that the existence of the CP will be associated with large event-by-event fluctuation of low momentum pions and suppressed fluctuation of T and μ_B . The non-monotonic dependence of multiplicity fluctuations on $\sqrt{s_{NN}}$ [17], the y dependence of cumulants of the event-by-event proton distributions [18] and the multiplicity fluctuations of pions and protons [19], appearance of negative kurtosis of the order parameter fluctuation [20] are some of the proposed signals of the CP (for a review see [21] and references therein).

Relativistic hydrodynamics (see [22, 23] for review and references therein) has been used extensively to analyze various experimental data originating from heavy ion collisions over a wide range of $\sqrt{s_{NN}}$ to extract properties of hot and dense QCD matter. It will be interesting to study how the hydrodynamic evolution of the QCD matter will be affected by the presence of CP. The effects of CP enter into the relativistic viscous hydrodynamics through the

*Correspondence email address: sushant7557@gmail.com

EoS and transport coefficients. The CP changes the EoS and various transport coefficients drastically. Therefore, it will be useful to examine the effects of CP on some of the observables *i.e.* the transverse momentum (p_T) distribution of the hadrons, the p_T and y dependence of flow coefficients.

We will use relativistic viscous causal hydrodynamics of Israel and Stewart with EoS containing the effect of CP and the scaling behaviour of shear and bulk viscosities near the CP. In a recent study we have found that the CP has the potential to substantially alter the spin polarization of hadrons [24]. In the present work we will investigate the response of the p_T and y distributions, directed and elliptic flow coefficients of hadrons (proton and pion) to the QCD critical point.

For this exercise, a numerical code in FORTRAN has been developed [from the scratch](#) to solve (3+1)-dimensional viscous relativistic causal hydrodynamics using the algorithm detailed in Ref. [25]. The code includes the effect of CP through the EoS and the scaling behaviour of the transport coefficients. The subroutines used for the initial condition and the EoS to solve hydrodynamic equations have been extensively tested by reproducing the results available in Refs. [26] and [27] respectively. The CORNELIUS code [28] has been used to find the freeze-out hypersurface characterized by constant energy density. The results from the code have been contrasted with the known analytical results of Ref. [29] and numerical results from the codes AZHYDRO [30], MUSIC [31] and vHLLE [25] by excluding the CP.

The paper is organized as follows. In section II the method for the numerical solution of hydrodynamic equations has been discussed. Relevant inputs *e.g.* the initial condition, equation of state (EoS), transport coefficients are presented through different subsections of this section. We present the results in section III and section IV is devoted to summary and discussions.

II. NUMERICAL SOLUTION OF RELATIVISTIC HYDRODYNAMICS

Throughout the paper we use natural units with $c = \hbar = k_B = 1$ where c is the speed of light in vacuum, \hbar ($= 2\pi\hbar$) is the Planck's constant and k_B is the Boltzmann's constant. The flat space time metric is taken as $g_{\mu\nu} = \text{diag}(1, -1, -1, -1)$.

A. Hydrodynamic Equations

The relativistic hydrodynamic equations governing the evolution of the system are:

$$\begin{aligned}\partial_\mu T^{\mu\nu} &= 0 \\ \partial_\mu J_B^\mu &= 0\end{aligned}\tag{1}$$

where $T^{\mu\nu}$ is the energy-momentum tensor and J_B^μ is the net-baryon number current. In the Landau frame, $T^{\mu\nu}$ and J_B^μ are given by

$$\begin{aligned}T^{\mu\nu} &= \varepsilon u^\mu u^\nu - (P + \Pi)\Delta^{\mu\nu} + \pi^{\mu\nu} \\ J_B^\mu &= n_B u^\mu + V^\mu\end{aligned}\tag{2}$$

where ε , n_B , P , u^μ , Π , $\pi^{\mu\nu}$, V^μ and $\Delta^{\mu\nu}(= g^{\mu\nu} - u^\mu u^\nu)$ denote respectively the energy density, net-baryon number density, thermodynamic pressure, four-velocity, bulk pressure, shear-stress tensor, baryon diffusion four-current and projector tensor onto the space orthogonal to u^μ . In the Israel-Stewart framework the viscous terms obey relaxation type equations which are taken as [25, 32]:

$$u^\gamma \partial_\gamma \Pi = -\frac{\Pi - \Pi_{NS}}{\tau_\Pi} - \frac{4}{3}\Pi \partial_\gamma u^\gamma\tag{4}$$

$$\langle u^\gamma \partial_\gamma \pi^{\mu\nu} \rangle = -\frac{\pi^{\mu\nu} - \pi_{NS}^{\mu\nu}}{\tau_\pi} - \frac{4}{3}\pi^{\mu\nu} \partial_\gamma u^\gamma\tag{5}$$

$$u^\gamma \partial_\gamma V^\mu = -\frac{V^\mu - V_{NS}^\mu}{\tau_V} - V^\mu \partial_\gamma u^\gamma\tag{6}$$

where $\langle \cdot \rangle$ is defined as

$$\langle A^{\mu\nu} \rangle = \left(\frac{1}{2}\Delta_\alpha^\mu \Delta_\beta^\nu + \frac{1}{2}\Delta_\alpha^\nu \Delta_\beta^\mu - \frac{1}{3}\Delta^{\mu\nu} \Delta_{\alpha\beta} \right) A^{\alpha\beta}$$

and Π_{NS} , $\pi_{NS}^{\mu\nu}$, V_{NS}^μ are the Navier-Stokes limit of Π , $\pi^{\mu\nu}$ and V^μ respectively and, are given by

$$\Pi_{NS} = -\zeta\theta \quad (7)$$

$$\pi_{NS}^{\mu\nu} = 2\eta \langle \partial^\alpha u^\beta \rangle \quad (8)$$

$$V_{NS}^\mu = \kappa_B \Delta^{\mu\nu} \partial_\nu \left(\frac{\mu_B}{T} \right) \quad (9)$$

The transport coefficients are positive *i.e.* $\eta, \zeta, \kappa_B > 0$ where η , ζ and κ_B are the shear viscosity, bulk viscosity and thermal conductivity respectively. In the present study we take $V^\mu = 0$. As mentioned above a numerical code has been developed in FORTRAN programming language to solve the hydrodynamic equations in Milne coordinates (τ, x, y, η_s) , using the relativistic HLL algorithm as in [25], where $\tau = \sqrt{t^2 - z^2}$ and $\eta_s = \tanh^{-1}(z/t)$. The various inputs to the numerical program needed for this study are detailed below.

B. Initial Condition

The Glauber model has been used to estimate the energy density profile at the initial time, τ_0 , required to solve the hydrodynamical equations. The value of τ_0 , for the hydrodynamic simulation is assumed as the time taken by the two colliding nuclei to pass through one another for $\sqrt{s_{NN}} \leq 24$ GeV which is determined by the following expression

$$\tau_0 \approx \frac{2R}{\gamma_z v_z},$$

where $\gamma_z = \frac{1}{\sqrt{1-v_z^2}}$ and $v_z = \tanh(y_b)$, with $y_b = \cosh^{-1}(\sqrt{s}/2m_N)$ as the beam rapidity, m_N is the mass of a nucleon and R is the radius of nucleus. The value of τ_0 is taken as 1 fm/c for $\sqrt{s_{NN}} > 24$ GeV.

The inelastic nucleon-nucleon cross-section (σ_{NN}^{in}) required as an input to the Glauber model as a function of the colliding energy \sqrt{s} (in GeV) is taken from the following parametrization [33, 34]:

$$\begin{aligned} \sigma_{NN}^{\text{tot}}(\sqrt{s}) &= 42.6s^{-0.46} - 33.4s^{-0.545} + 35.5 \\ &\quad + 0.307 \ln^2(s/29.1) \\ \sigma_{NN}^{\text{el}}(\sqrt{s}) &= 5.17 + 12.99s^{-0.41} + 0.09 \ln^2(s/29.2) \\ \sigma_{NN}^{\text{in}}(\sqrt{s}) &= \sigma_{NN}^{\text{tot}} - \sigma_{NN}^{\text{el}} \end{aligned}$$

Our model for the initial condition is based on the inputs taken from [26, 32]. The collision axis is assumed to be along the z -axis. Let n_A and n_B denote the number of wounded nucleons per unit area in the transverse plane of the two colliding nuclei A and B , respectively moving along the positive and negative z -axis. The n_A (n_B) is given by

$$n_{A,B} = T_{A,B} \left[1 - \left(1 - \frac{\sigma_{NN}^{\text{in}} T_{B,A}}{N_{B,A}} \right)^{N_{B,A}} \right]. \quad (10)$$

where N_A and N_B denote the total number of nucleons in A and B , respectively, and the thickness functions $T_A(x, y)$ and $T_B(x, y)$ are calculated as follows:

$$T_{A,B}(x, y) = \int_{-\infty}^{\infty} \varrho_{A,B}(x, y, z') dz', \quad (11)$$

where $\varrho_{A,B}(x, y, z)$ is the nuclear density profile assumed to have the Woods-Saxon shape,

$$\varrho_{A,B}(x, y, z) = \frac{\varrho_0}{1 + e^{\frac{r-R(\theta)}{\delta}}}. \quad (12)$$

The constant ϱ_0 is chosen to satisfy the relation:

$$\int \varrho_i(\vec{r}) d^3\vec{r} = N_i, \quad i = A, B \quad (13)$$

and $R(\theta)$ has been taken as a function of the polar angle, θ , to account for any deformation of the nucleus, and is given by

$$R(\theta) = R_0 [1 + \beta_2 Y_{2,0}(\theta) + \beta_4 Y_{4,0}(\theta)] \quad (14)$$

where $Y_{l,m}(\theta, \phi)$ denotes the spherical harmonics. In this study, we consider nuclei to be spherical and take $\beta_2, \beta_4 = 0$. For gold (Au) nucleus, R_0 is taken as 6.37 fm. The initial energy density is assumed to have the following form

$$\varepsilon(x, y, \eta_s; \tau_0) = e(x, y) f(\eta_s) \quad (15)$$

where $f(\eta_s)$ is given by [26]

$$f(\eta_s) = \exp \left[-\frac{(|\eta_s - y_{\text{CM}}| - \eta_0)^2}{2\sigma_\eta^2} \theta(|\eta_s - y_{\text{CM}}| - \eta_0) \right]. \quad (16)$$

where

$$y_{\text{CM}} = \text{arctanh} \left[\frac{n_A - n_B}{n_A + n_B} \tanh(y_b) \right]$$

and $e(x, y) = \mathcal{N}_e M(x, y)$ with

$$M(x, y) = m_N \sqrt{n_A^2 + n_B^2 + 2n_A n_B \cosh(2y_b)}.$$

The normalization constant \mathcal{N}_e is determined by demanding local energy-momentum conservation [26]. The following profile for the initial velocity distribution is assumed here,

$$w^\mu(x, y, \eta_s) = (\cosh(\eta_s), 0, 0, \sinh(\eta_s)). \quad (17)$$

We take the following profile for the initial baryon density,

$$n_B(x, y, \eta_s; \tau_0) = \mathcal{N}_B [g_A(\eta_s)n_A(x, y) + g_B(\eta_s)n_B(x, y)] \quad (18)$$

where $g_A(\eta_s)$ and $g_B(\eta_s)$ are given by [32]

$$\begin{aligned} g_A(\eta_s) &= \theta(\eta_s - \eta_{B,0}) \exp \left[-\frac{(\eta_s - \eta_{B,0})^2}{2\sigma_{B,\text{out}}^2} \right] \\ &\quad + \theta(\eta_{B,0} - \eta_s) \exp \left[-\frac{(\eta_s - \eta_{B,0})^2}{2\sigma_{B,\text{in}}^2} \right] \\ g_B(\eta_s) &= \theta(\eta_s + \eta_{B,0}) \exp \left[-\frac{(\eta_s + \eta_{B,0})^2}{2\sigma_{B,\text{in}}^2} \right] \\ &\quad + \theta(-\eta_{B,0} - \eta_s) \exp \left[-\frac{(\eta_s + \eta_{B,0})^2}{2\sigma_{B,\text{out}}^2} \right] \end{aligned}$$

and \mathcal{N}_B is fixed by the condition

$$\begin{aligned} \int \tau_0 dx dy d\eta_s n_B(x, y, \eta_s; \tau_0) &= N_{\text{part}} \\ \Rightarrow \int d\eta_s n_B(x, y, \eta_s; \tau_0) &= \frac{1}{\tau_0} [n_A(x, y) + n_B(x, y)] \end{aligned}$$

which gives

$$\mathcal{N}_B = \frac{1}{\tau_0} \sqrt{\frac{2}{\pi} \frac{1}{\sigma_{B,\text{in}} + \sigma_{B,\text{out}}}}. \quad (19)$$

The initial condition, hence, is modeled through 6 parameters, $(\tau_0, \eta_0, \sigma_\eta, \eta_{B,0}, \sigma_{B,\text{in}}, \sigma_{B,\text{out}})$ which are chosen from Ref [26] for Au+Au collisions.

C. Equation of State

The EoS has been obtained by following the procedure detailed in Ref [27] by assuming that the CP in QCD belongs to the same universality class as that of 3D Ising model. The procedure is briefly reviewed below. The pressure at non-zero T and μ_B can be obtained through a Taylor series expansion about $\mu_B = 0$ as follows

$$P_{\text{QCD}}(T, \mu_B) = T^4 \sum_n c_{2n}(T) \left(\frac{\mu_B}{T}\right)^{2n}, \quad (20)$$

where

$$c_n(T) = \frac{1}{n!} \left. \frac{\partial^n (P/T^4)}{\partial (\mu_B/T)^n} \right|_{\mu_B=0} = \frac{1}{n!} \chi_n(T). \quad (21)$$

If there were no singularity, then the series expansion given in Eq.(20) would have been valid throughout the QCD phase diagram. However, the presence of CP makes some of the coefficients diverge. Hence the pressure can be written as a sum of a regular and a singular part. Equivalently, the expansion coefficients in Eq.(20) are replaced by

$$T^4 c_n(T) \rightarrow T^4 c_n^{\text{Non-Ising}}(T) + f(T, \mu_B) c_n^{\text{Ising}}(T). \quad (22)$$

where the superscript ‘‘Non-Ising’’ and ‘‘Ising’’ represent the regular and the singular (or critical) contributions respectively. $f(T, \mu_B)$ is chosen so that it does not add any other singularity in the problem, and can simply be chosen as

$$f(T, \mu_B) = T_c^4.$$

The critical part is obtained by using the 3D Ising model because the QCD critical point belongs to the same universality class as the 3D Ising model. Hence, the two models must show the same scaling behavior in the critical region. The critical exponents of the 3D Ising model are known through numerical simulations. Hence, by mapping the parameters of the two systems in the critical region, it is possible to extract the critical behavior of QCD near T_c . The mapping from the Ising model phase diagram (r, h) to the QCD phase diagram (μ_B, T) is done with the help of the following relations:

$$\begin{aligned} \frac{T - T_C}{T_C} &= w (r \rho \sin \alpha_1 + h \sin \alpha_2), \\ \frac{\mu_B - \mu_{BC}}{T_C} &= w (-r \rho \cos \alpha_1 - h \cos \alpha_2), \end{aligned} \quad (23)$$

The Ising pressure in the critical region is given by

$$P_{\text{Ising}}(R, \theta) = h_0 M_0 R^{2-\alpha} \left[\theta \tilde{h}(\theta) - g(\theta) \right] \quad (24)$$

where $\tilde{h}(\theta) = \theta(1 + a\theta^2 + b\theta^4)$, $g(\theta) = c_0 + c_1(1 - \theta^2) + c_2(1 - \theta^2)^2 + c_3(1 - \theta^2)^3$; $h_0, M_0, a, b, c_0, c_1, c_2, c_3$ are constants, some given in terms of critical exponents. (R, θ) are related to (r, h) through the following transformations

$$h = h_0 R^{\beta\delta} \tilde{h}(\theta) \quad (25)$$

$$r = R(1 - \theta^2) \quad (26)$$

where β and δ are critical exponents. Hence the coefficients contributing to the critical part are determined through

$$c_n^{\text{Ising}}(T) = \frac{1}{n!} T^n \left. \frac{\partial^n P^{\text{Ising}}}{\partial \mu_B^n} \right|_{\mu_B=0}, \quad (27)$$

The ‘‘Non-Ising’’ coefficients are chosen in such a way that at $\mu_B = 0$, the expansion coefficients so obtained match the results obtained from LQCD *i.e.*

$$T^4 c_n^{\text{LAT}}(T) = T^4 c_n^{\text{Non-Ising}}(T) + f(T, \mu_B = 0) c_n^{\text{Ising}}(T). \quad (28)$$

Having determined the “Ising” and “Non-Ising” coefficients, the full pressure is then obtained as

$$P_{\text{QCD}}(T, \mu_B) = T^4 \sum_n c_{2n}^{\text{Non-Ising}}(T) \left(\frac{\mu_B}{T}\right)^{2n} + T_c^4 P^{\text{Ising}}(R(T, \mu_B), \theta(T, \mu_B)). \quad (29)$$

The procedure as detailed above gives various thermodynamic observables as a function of T and μ_B . However, for our numerical hydrodynamic code we require pressure (P) as a function of energy density (ε) and baryon number density (n_B). To construct such a table, we follow a procedure similar to [35]. The $\varepsilon - n_B$ plane is discretized with the following scheme,

$$\Delta\varepsilon \text{ (GeV/fm}^3\text{)} = \begin{cases} 0.002 & \text{if } 0.001 \leq \varepsilon < 1.001 \\ 0.02 & \text{if } 1.001 \leq \varepsilon < 11.001 \\ 0.1 & \text{if } 11.001 \leq \varepsilon < 61.001 \\ 0.5 & \text{if } 61.001 \leq \varepsilon < 101.001 \end{cases}$$

$$\Delta n_B \text{ (fm}^{-3}\text{)} = \begin{cases} 0.0005 & \text{if } 0 \leq n_B < 0.15 \\ 0.001 & \text{if } 0.15 \leq n_B < 0.3 \\ 0.01 & \text{if } 0.3 \leq n_B < 1 \\ 0.025 & \text{if } 1 \leq n_B < 5 \end{cases}$$

Small value for discretization is chosen to correctly reproduce the critical behavior and discontinuity in thermodynamic quantities due to the first-order transition beyond the critical point. For other values of (ε, n_B) , the pressure and other thermodynamic variables are obtained through 2D linear interpolation. For all those (ε, n_B) where T and μ_B lies outside the range (5, 450) MeV and (0, 450) MeV respectively, the thermodynamic variables are put to zero.

D. Transport Coefficients

Before providing expressions for the transport coefficients we shall give an account of how the equilibrium correlation length can be obtained with an equation of state near the CP. The procedure of Ref.[36] has been followed to calculate the equilibrium correlation length ξ . ξ is computed in the Ising model by taking derivative of equilibrium magnetization, $M(r, h)$, with respect to h at fixed r as follows

$$\xi^2 = \frac{1}{H_0} \left(\frac{\partial M(r, h)}{\partial h} \right)_r$$

where H_0 is a dimensionful parameter to get the correct dimensions of ξ . We shall take $H_0 = 1$ in our calculations. In fact, the derivative of $M(r, h)$ with respect to h is the

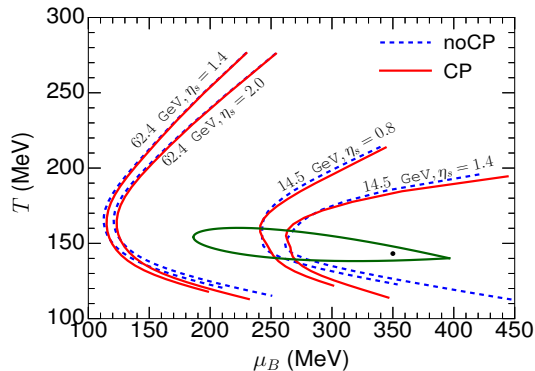


FIG. 1: Trajectory traced by the fluid cell at $x = y = 0$ in the $T - \mu_B$ plane for different space-time rapidities, two colliding energies (14.5 GeV and 62.4 GeV) and for impact parameter $b = 5$ fm. The critical point is indicated in solid black dot at $(T, \mu_B) = (350, 143.2)$ MeV and the boundary of the critical region is indicated by the solid green line.

magnetic susceptibility (χ_M) in the Ising model which, near a critical point, goes as $\xi^{2-\eta'}$, where the value of η' is found to be small ($\eta' \approx 0.036$). In this work we have taken $\eta' = 0$. The equilibrium magnetization is parametrized in terms of variables R and θ as

$$M(R, \theta) = M_0 R^\beta \theta$$

where R and θ are related to r and h through Eqns.(25) and (26). Now using the identity

$$\left(\frac{\partial M}{\partial h}\right)_r = \left(\frac{\partial M}{\partial R}\right)_\theta \left(\frac{\partial R}{\partial h}\right)_r + \left(\frac{\partial M}{\partial \theta}\right)_R \left(\frac{\partial \theta}{\partial h}\right)_r$$

and the expressions for $\left(\frac{\partial R}{\partial h}\right)_r$ and $\left(\frac{\partial \theta}{\partial h}\right)_r$ given in Ref.[27], we have

$$\xi^2 = \frac{M_0}{h_0} \frac{R^{\beta(1-\delta)}}{2\beta\delta\theta\dot{h}(\theta) + (1-\theta^2)\dot{h}'(\theta)} [1 + (2\beta - 1)\theta^2] \quad (30)$$

Near the critical point, the transport coefficients are expected to vary with the correlation length as follows

$$\zeta \sim \xi^3, \quad \eta \sim \xi^{0.05}, \quad \kappa_T \sim \xi$$

We define the region in the $\mu_B - T$ plane bounded by the curve $\xi(\mu_B, T) = \xi_0$ as the critical region *i.e.* for $\xi < \xi_0$, the transport coefficients are regular functions of T and μ_B but for $\xi > \xi_0$, the transport coefficients must satisfy the scaling laws as defined above. We choose $\xi_0 = 1.75$ fm. In this work, we only consider bulk viscosity (ζ) and shear viscosity (η). The critical behavior of these transport coefficients can then be modeled as

$$\zeta = \zeta_0 \left(\frac{\xi}{\xi_0}\right)^3, \quad \eta = \eta_0 \left(\frac{\xi}{\xi_0}\right)^{0.05} \quad (31)$$

where ζ_0, η_0 denote the values outside the critical region which are chosen as[32, 37]

$$\eta_0(\mu_B, T) = 0.08 \left(\frac{\varepsilon + p}{T}\right)$$

$$\zeta_0(\mu_B, T) = 15 \eta_0(\mu_B, T) \left(\frac{1}{3} - c_s^2\right)^2$$

The relaxation times in Eqs.(4) and (5) also diverge near the critical point. This is included by using the following expressions for the relaxation times

$$\tau_\pi = \tau_\pi^0 \left(\frac{\xi}{\xi_0}\right)^{0.05}, \quad \tau_\Pi = \tau_\Pi^0 \left(\frac{\xi}{\xi_0}\right)^3. \quad (32)$$

where τ_π^0 and τ_Π^0 are the relaxation times outside the critical region, which we take as follows (with $C_\eta = 0.08$) [38],

$$\frac{\tau_\pi^0}{5} = \tau_\Pi^0 = \frac{C_\eta}{T}.$$

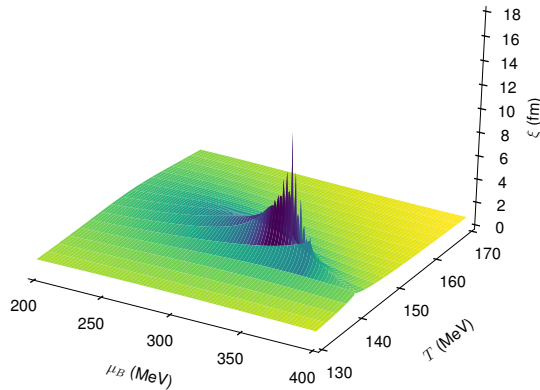


FIG. 2: Correlation length, ξ , plotted as a function of μ_B and T .

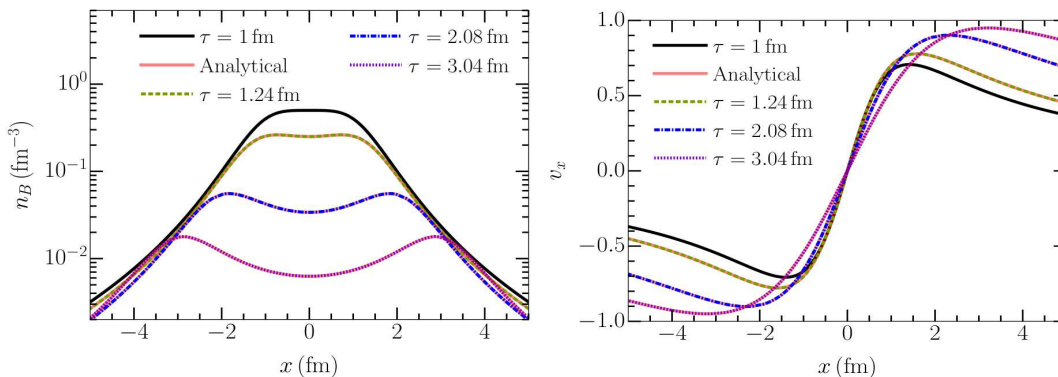


FIG. 3: Comparison of the code output with analytic Gubser solution. The results are plotted at $y = 0$ after setting $q = 1$ in Eqs.(35) and (36).

The critical domain is delineated in $\mu_B - T$ plane by setting $\xi(\mu_B, T) = \xi_0 = 1.75$ fm. The critical point indicated by black dot and the critical domain enclosed by the green line are shown in Fig.(1). The trajectories of the system in $\mu_B - T$ plane formed at two $\sqrt{s_{NN}}$ with and without CP have been displayed. The trajectories of the fluid cells at lower $\sqrt{s_{NN}}$ pass through the critical region but for higher $\sqrt{s_{NN}}$ the trajectories remain away from the critical region. But for a fixed collision energy, the fluid cell at larger space-time rapidity, η_s , lies closer to the critical point and will feel the effect of EoS and enhanced values of transport coefficients more. The evolution of fluid cell at $(x, y, \eta_s) = (0, 0, 1.4)$ at $\sqrt{s_{NN}} = 14.5$ GeV is displayed in Fig.(1). The results clearly show that the trajectories at higher η_s get attracted towards the critical point.

The correlation length as obtained in Eq.(30) is shown in Fig.(2) as function of μ_B and T . The drastic increase in ξ in the vicinity of the CP is conspicuous due to the divergent nature of the transport coefficients.

E. Numerical implementation

We perform the hydrodynamical simulation on a $201 \times 201 \times 71$ space grid such that $\Delta x = \Delta y = \Delta \eta = 0.2$ fm. Also time step for the evolution is chosen as $\Delta \tau = 0.05$ fm. This choice satisfies the CFL (Courant-Friedrichs-Lewy) criterion for the stability of the code. Further the time evolved quantities are written to a data file after evolving for 0.5 fm time from the previous step. We use CORNELIUS [28] code to find a constant energy density surface within a computational (fluid) cell. The CORNELIUS code provides the coordinates $(\tau_f, x_f, y_f, \eta_{sf})$ and area elements $d\Sigma_\nu$ of the freeze-out surface. The quantities like T, ε etc at $(\tau_f, x_f, y_f, \eta_{sf})$ are calculated through 2D linear interpolation using the values at the corners of the cell. We shall analyze the effects of the CP on the surface $\varepsilon = 0.3$ GeV/fm³, henceforth denoted as Σ_{CFO} . The aim here is not to compare and reproduce the experimental data but to pinpoint the effects that CP will induce on various hydrodynamic quantities and hence on the experimental observables.

We calculate the space averaged quantity, say transverse velocity, $v_T = \sqrt{v_x^2 + v_y^2}$ by using the following expression:

$$\langle v_T \rangle (\tau) = \frac{\int d^3x \varepsilon(\tau, x, y, \eta_s) v_T(\tau, x, y, \eta_s)}{\int d^3x \varepsilon(\tau, x, y, \eta_s)}$$

where $\varepsilon(\tau, x, y, \eta_s)$ is the energy density. The p_T spectrum of the hadrons, $\frac{dN}{d^2p_T dy}$ can be calculated by using the Cooper-Frye formula as:

$$\frac{dN_i}{d^2p_T dy} = \frac{g_i}{(2\pi)^3} \int d\sigma_\mu p^\mu f_i(x, p)$$

where $f_i(x, p)$ is given by

$$f_i(x, p) = \frac{1}{e^{(p^\mu u_\mu - \mu_{B,F})/T_F} + a_i}$$

where T_F and $\mu_{B,F}$ denote the temperature and chemical potential on the surface Σ_{CFO} , $a_i = -1$ for bosonic statistics, $a_i = +1$ for fermionic statistics and $a_i = 0$ for classical (Boltzmann) statistics. We do not consider a viscous correction (δf_i) to the distribution f_i in evaluating $\frac{dN_i}{d^2p_T dy}$ as the effect may not be significant [36].

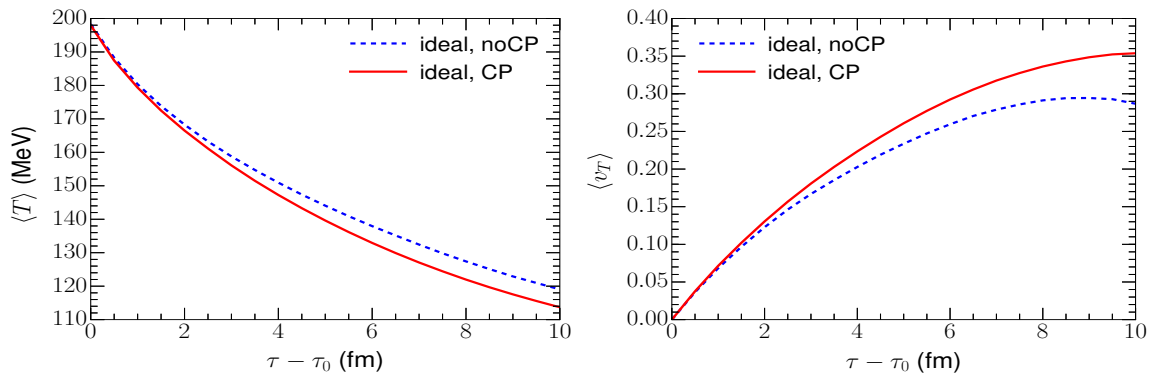


FIG. 4: Time evolution of (left) average temperature, and (right) transverse velocity using ideal hydrodynamics and EoS with (CP, red solid line) and without (noCP, blue dashed line) the critical point for Au+Au collision at $\sqrt{s_{NN}} = 14.5$ and impact parameter $b = 5$ fm.

The other experimental measurable quantities, like flow coefficients are calculated by using the following expression,

$$v_n(p_T, y) = \frac{\int d\phi \frac{dN}{d^2p_T dy} \cos(n\phi)}{\int d\phi \frac{dN}{d^2p_T dy}} \quad (33)$$

The p_T -integrated flow coefficient is obtained as

$$v_n(y) = \int_{p_{T,min}}^{p_{T,max}} dp_T v_n(p_T, y)$$

where we take $p_{T,min} = 0.2$ GeV and $p_{T,max} = 3$ GeV. Similarly, the rapidity integrated flow coefficient is obtained as

$$v_n(p_T) = \int_{y_{min}}^{y_{max}} dy v_n(p_T, y)$$

where we have chosen $y_{min} = -1$ and $y_{max} = 1$.

III. RESULTS AND DISCUSSIONS

We compare numerical results from our code and the analytical Gubser solution in Fig.(3). The Gubser solution is given by [29, 32]

$$\varepsilon(\tau, r) = \frac{\varepsilon_0}{\tau^4} \frac{(2q\tau)^{8/3}}{\left[1 + 2(\tau^2 + r^2) + (\tau^2 - r^2)^2\right]^{4/3}} \quad (34)$$

$$n_B(\tau, r) = \frac{n_{B0}}{\tau^3} \frac{(2q\tau)^2}{\left[1 + 2(\tau^2 + r^2) + (\tau^2 - r^2)^2\right]} \quad (35)$$

$$v_x(\tau, r) = \frac{2q^2\tau x}{1 + q^2r^2 + q^2\tau^2} \quad (36)$$

$$v_y(\tau, r) = \frac{2q^2\tau y}{1 + q^2r^2 + q^2\tau^2} \quad (37)$$

where $r = \sqrt{x^2 + y^2}$. The numerical solution is in perfect agreement with the analytical result. Next we show the time evolution of the average temperature of the fireball formed in Au+Au collisions ($\sqrt{s_{NN}} = 14.5$ GeV at impact parameter $b = 5$ fm) in Fig.(4) using the ideal hydrodynamics (all transport coefficients set to zero) and EoS with (red solid line) and without (blue dashed line) the critical point. For a given initial condition, the addition of the critical part to the regular pressure leads to a larger value of the net pressure, and hence a large gradient of the pressure with

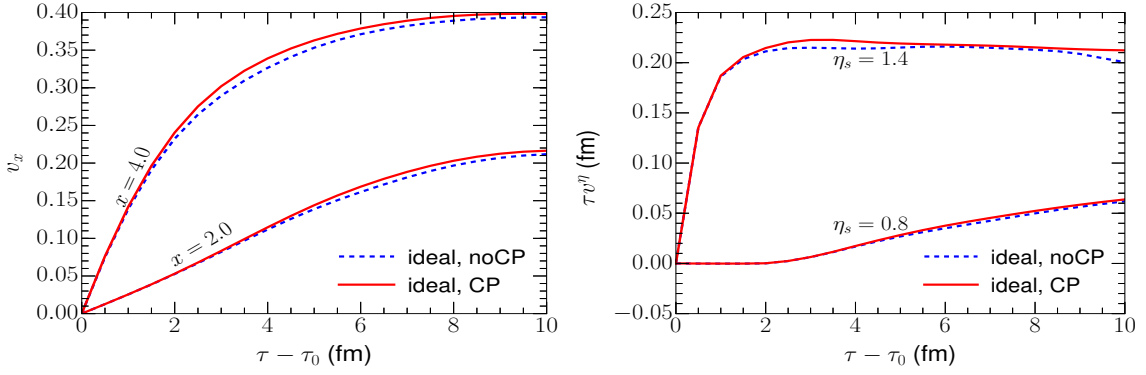


FIG. 6: (left) Time evolution of v_x for the fluid cell at $y = 0$, $\eta_s = 0$ at different x and (right) time evolution of v_η for the fluid cell at $x = y = 0$ at different space-time rapidities for Au+Au collision at $\sqrt{s_{NN}} = 14.5$ and impact parameter $b = 5$ fm.

respect to the vacuum outside. This leads to a faster expansion and a faster rate of cooling as shown in the left panel of Fig.(4). Higher pressure introduced by the CP lead to higher flow too as reflected in v_T , as shown in the right panel of Fig.(4).

In Fig.(5), we show the time evolution for v_x of a fluid cell at different space-time rapidities for Au+Au collision at $\sqrt{s_{NN}} = 14.5$ and impact parameter $b = 5$ fm. The results indicate that a gradient of v_x along the η_s -direction is generated which is due to our choice of tilted initial condition. The presence of CP marginally increases this gradient.

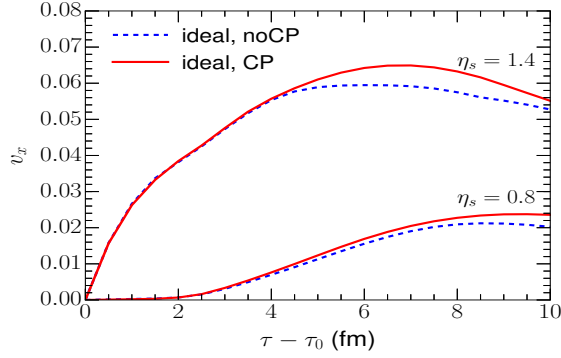


FIG. 5: Time evolution for x -component of velocity (v_x) of the fluid cell at $x = y = 0$ and at different space-time rapidities for Au+Au collision at $\sqrt{s_{NN}} = 14.5$ and impact parameter $b = 5$ fm.

Similarly, the transverse and longitudinal expansions also increases marginally due to the presence of the critical point for ideal hydrodynamics as shown in Fig.(6). It should, however, to be noted that the profile is mostly monotonic.

Now we discuss results with the inclusion of the viscous effects in the QGP fluid. As the viscous fireball of QGP expands, the fluid cells towards the boundary, which are closer to the critical region, undergo slower expansion due to enhanced viscosity. The expansion of the fluid cells in the bulk is not strongly affected by the critical point. This leads to the buildup of matter somewhere in between, due to which the expansion results in a non-monotonic profile. This is reflected in the variation of v_x with τ for different values of x (Figs.7) and η_s (left panel of Fig. 8). The variation of τv_η with τ for different values of η_s display similar nature (right panel of 8). The non-monotonicity is prominent for larger values of η_s which corresponds to the evolution trajectory closer to the CP (see Fig. 1. The effect of CP on v_x at $\eta_s = 1.4$ gives rise to a horn like structure. We will check below whether such structure survives in the space-time integrated observables. It is to be stressed further that as the critical point is approached, these effects get enhanced. To further confirm this argument, we also show the velocity profile for $\sqrt{s_{NN}} = 62.4$ GeV in Fig.(9). The trajectories in this case are far away from the critical region and thus the effects of EoS and enhanced viscosities are small. Therefore, the non-monotonicity observed in the time evolution of v_x and τv_η can be attributed to the CP. However, it will be interesting to examine whether such effects of CP survives in experimental observables like p_T spectra and various flow coefficients which are obtained by integrating over the entire space-time history of the fireball. This exercise has been carried out below.

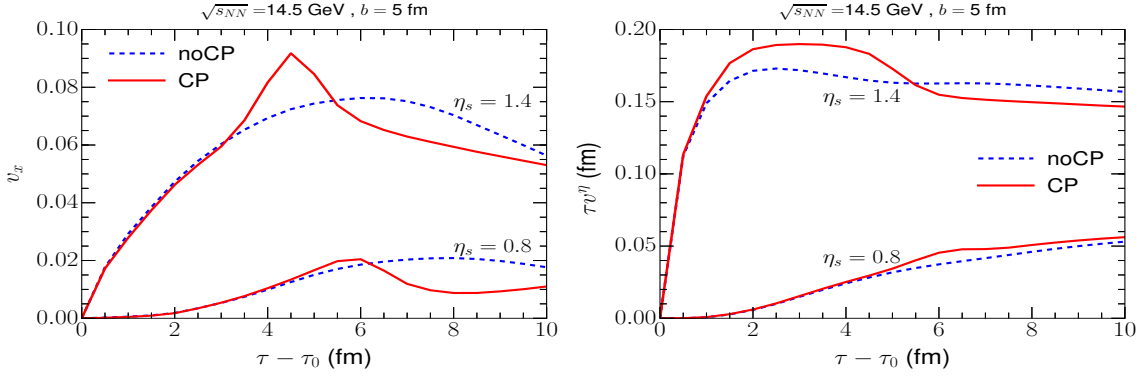


FIG. 8: Time evolution of v_x at different values of x (left panel) and τv_η at different η_s for the fluid cell at $x = y = 0$, for $\sqrt{s_{NN}} = 14.5$ GeV and $b = 5$ fm.

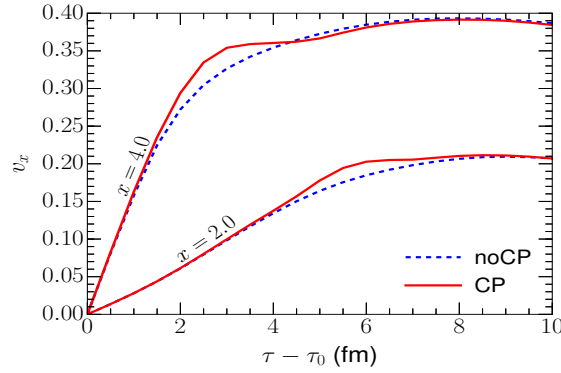


FIG. 7: Time evolution of v_x at different x for the fluid cell at $y = 0$, $\eta_s = 0$ for $\sqrt{s_{NN}} = 14.5$ GeV and $b = 5$ fm.

It is clear that the effects of the CP through the EoS and transport coefficients do not affect the velocity much but it surely affects the gradients of velocity profile.

We have evaluated the p_T spectra, directed and elliptic flow coefficients of pion and proton with the inclusion of the effects of CP on the EoS and transport coefficients. The p_T spectra of π^+ and proton have been displayed in Fig. 10) for two colliding energies *i.e.* $\sqrt{s_{NN}} = 14$ GeV (left panel) 62.4 GeV (right panel). The rapidity distribution of pion and proton are shown in Fig.11 for two colliding energies *i.e.* $\sqrt{s_{NN}} = 14.5$ GeV and $\sqrt{s_{NN}} = 62.4$ GeV, no distinguishable effect of CP is found. The effects of CP on the spectra is found to be insignificant because both the p_T and y distributions are obtained by integration over the space-time evolution history of the fireball produced in these collisions, *i.e.* results are superposition of all the temperatures and densities through which the system passes, it does not depend on the point, (μ_c, T_c) alone.

The rapidity distribution of v_1 of proton and pion are displayed in Fig. (12) as a function of y for $\sqrt{s_{NN}} = 14$ GeV and 62.4 GeV. The effects of CP both on π^+ and proton are seen to be insignificant as expected. The elliptic flow of both protons and π^+ increases marginally around $p_T \sim 2$ GeV compared to the case when there is no CP (left panel of Fig. 13) for $\sqrt{s_{NN}} = 14.5$ GeV. For $\sqrt{s_{NN}} = 62.4$ GeV, there is no shift in v_2 due to the inclusion of CP (right panel of Fig. 13) which is expected because the trajectory in this case remain away from the critical domain.

A faster expansion leads to a rapid fall in temperature and chemical potential which leads to a slight reduction in the yield of both π^+ and protons as shown in Fig.(10). These effects will definitely get enhanced as we approach the critical point. However, within the current model, the effect is only marginal and might not even be detected experimentally. As it has been shown in Ref. [24] that the thermal vorticity which depends on the velocity gradient of the fluid is suppressed by the presence of CP. Consequently the rapidity dependence of the spin polarization of the Λ hyperon was shown to be drastically affected by the CP due to the coupling of the spin with the thermal vorticity. The CP may be detected by measuring the rapidity distribution of the spin polarization by tuning the beam energy. Therefore, one expect that those observables which depend on the gradient of velocity will be efficient signatures of the CP.

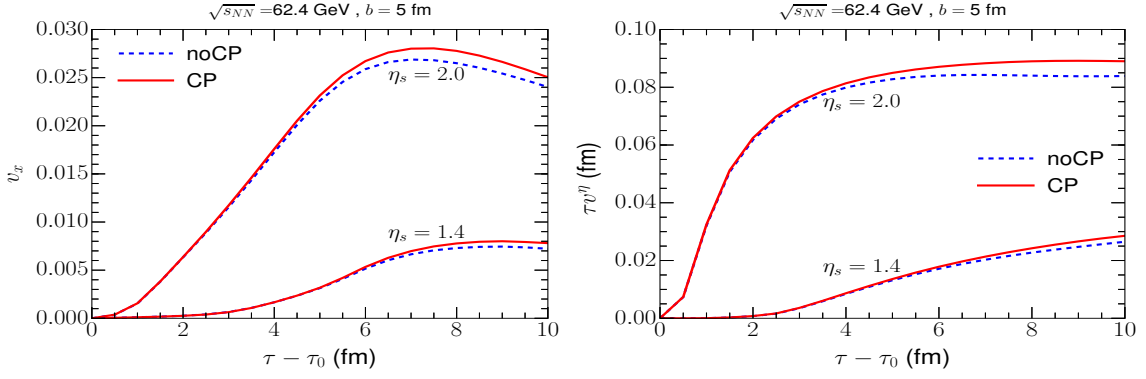


FIG. 9: Same as Fig. 8 for $\sqrt{s_{NN}} = 62.5$ GeV.

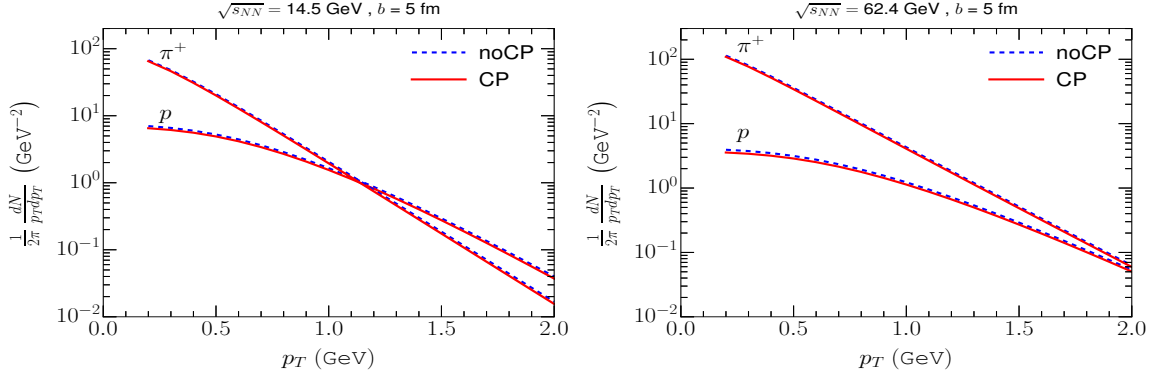


FIG. 10: Transverse momentum spectra is obtained by integrating ϕ and rapidity (y) between $-1 < y < 1$ for $\sqrt{s_{NN}} = 14.5$ (left panel) and 62.4 GeV (right panel).

IV. SUMMARY AND CONCLUSIONS

We have developed a computer code to solve the relativistic viscous causal hydrodynamics in (3+1) dimension. The effects of the QCD critical point (CP) have been included in the code through the equation of state and scaling behaviour of the transport coefficients. We study the evolution of the fireball of quarks and gluons formed at different values of μ_B and T corresponding to various values of $\sqrt{s_{NN}}$. The p_T spectra, directed and elliptic flow coefficients of pions and protons have been evaluated to understand the effects of CP on these quantities. We find that the integration over the entire space-time history of the fireball mostly wipe out the effects of CP on the spectra and flow

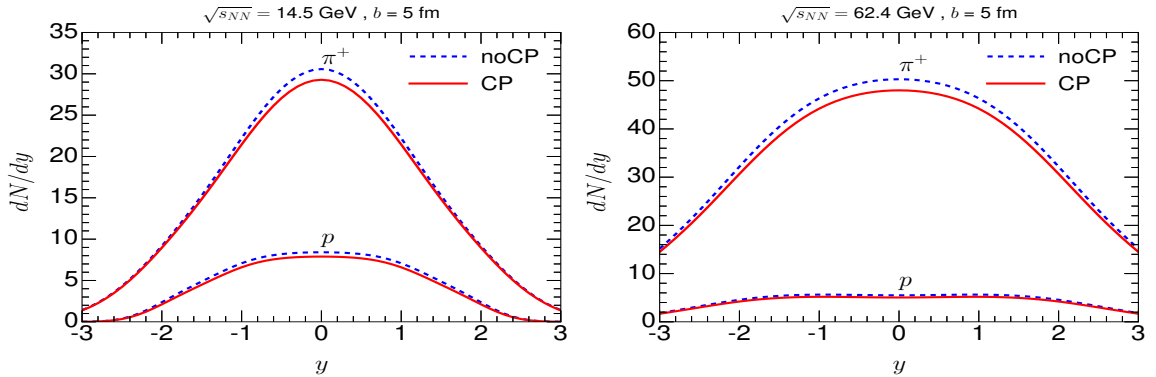


FIG. 11: The rapidity distribution of pion and proton for $\sqrt{s_{NN}} = 14.5$ (left panel) and 62.4 GeV (right panel).

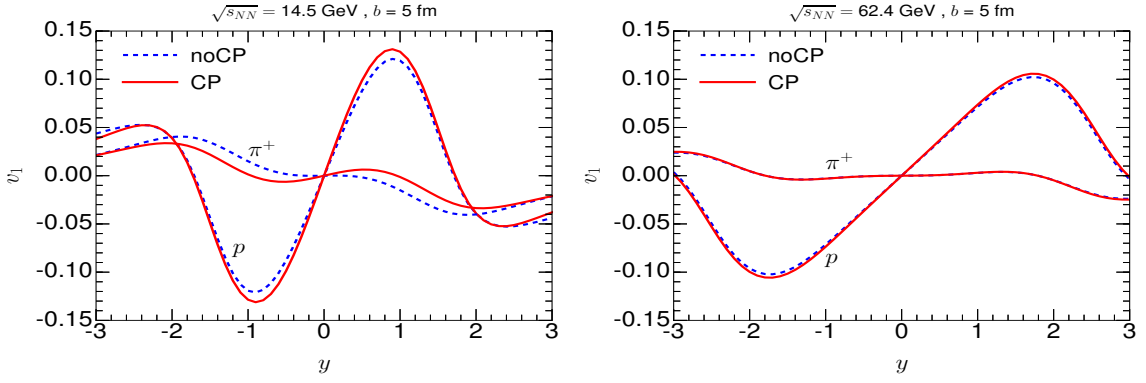


FIG. 12: Rapidity dependence of directed flow for two colliding energies (14.5 GeV and 62.4 GeV) and for impact parameter $b = 5$ fm.

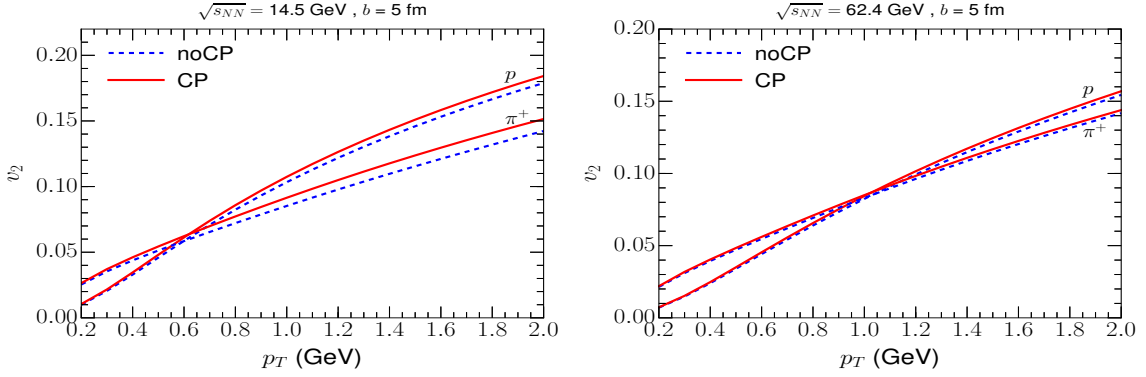


FIG. 13: p_T dependence of elliptic flow for two colliding energies (14.5 GeV and 62.4 GeV) and for impact parameter $b = 5$ fm.

coefficients which indicates that the detection of CP by using the hadronic spectra may not be useful. As the CP has the potential to substantially alter the rapidity distribution of spin polarization of hadrons, the measurement of spin polarization as a function of rapidity can be considered as an efficient tool to detect the CP [24].

A few comments on the validity of hydrodynamics near the CP are in order at this point. It is well-known that the fluid dynamics becomes invalid, because the fluctuating modes near the CP do not relax faster than the time scale of changes in slow/conserved variables due to which the local thermal equilibrium can not be maintained. However, the results obtained in this work may be considered as reasonable because of the following reasons. Firstly, the validity of the fluid dynamics can be extended by adding a scalar field representing the slow non-hydrodynamic modes connected to the relaxation rate of the critical fluctuation (see [39] and [40] for details). In a simple picture describing the evolution of a system near the CP, it has been explicitly shown that the modes associated with the scalar fields lags behind the hydrodynamic modes resulting in back reactions on the hydrodynamic variables, however, it was found that the back reaction has negligible effects on the hydrodynamic variables [41]. Secondly, one may recall that if a system is not too close to CP then hydrodynamics can still be applied in a domain around the CP [42].

-
- [1] A. Bazavov, F. Karsch, S. Mukherjee, and P. Petreczky (USQCD), Eur. Phys. J. A **55**, 194 (2019), arXiv:1904.09951 [hep-lat].
- [2] Z. Fodor and S. D. Katz, JHEP **03**, 014, arXiv:hep-lat/0106002.
- [3] M. Asakawa and K. Yazaki, Nucl. Phys. A **504**, 668 (1989).
- [4] A. M. Halasz, A. D. Jackson, R. E. Shrock, M. A. Stephanov, and J. J. M. Verbaarschot, Phys. Rev. D **58**, 096007 (1998), arXiv:hep-ph/9804290.
- [5] P. de Forcrand and O. Philipsen, Nucl. Phys. B **642**, 290 (2002), arXiv:hep-lat/0205016.
- [6] Y. Aoki, G. Endrodi, Z. Fodor, S. D. Katz, and K. K. Szabo, Nature **443**, 675 (2006), arXiv:hep-lat/0611014.
- [7] G. Endrodi, Z. Fodor, S. D. Katz, and K. K. Szabo, JHEP **04**, 001, arXiv:1102.1356 [hep-lat].

- [8] Z. Fodor and S. D. Katz, JHEP **04**, 050, arXiv:hep-lat/0402006 .
- [9] H.-T. Ding, F. Karsch, and S. Mukherjee, Int. J. Mod. Phys. E **24**, 1530007 (2015), arXiv:1504.05274 [hep-lat] .
- [10] R. V. Gavai, Pramana **84**, 757 (2015), arXiv:1404.6615 [hep-ph] .
- [11] P. Deb, A. Bhattacharyya, S. K. Ghosh, R. Ray, and A. Lahiri, Nucl. Phys. A **862-863**, 267 (2011), arXiv:1101.5228 [hep-ph] .
- [12] B.-J. Schaefer, J. M. Pawłowski, and J. Wambach, Phys. Rev. D **76**, 074023 (2007), arXiv:0704.3234 [hep-ph] .
- [13] T. K. Herbst, J. M. Pawłowski, and B.-J. Schaefer, Phys. Lett. B **696**, 58 (2011), arXiv:1008.0081 [hep-ph] .
- [14] J. Wambach, B.-J. Schaefer, and M. Wagner, Acta Phys. Polon. Supp. **3**, 691 (2010), arXiv:0911.0296 [hep-ph] .
- [15] O. DeWolfe, S. S. Gubser, and C. Rosen, Phys. Rev. D **83**, 086005 (2011), arXiv:1012.1864 [hep-th] .
- [16] M. A. Stephanov, K. Rajagopal, and E. V. Shuryak, Phys. Rev. Lett. **81**, 4816 (1998), arXiv:hep-ph/9806219 .
- [17] X. Luo and N. Xu, Nucl. Sci. Tech. **28**, 112 (2017), arXiv:1701.02105 [nucl-ex] .
- [18] J. Brewer, S. Mukherjee, K. Rajagopal, and Y. Yin, Phys. Rev. C **98**, 061901 (2018), arXiv:1804.10215 [hep-ph] .
- [19] M. A. Stephanov, Phys. Rev. Lett. **102**, 032301 (2009), arXiv:0809.3450 [hep-ph] .
- [20] M. A. Stephanov, Phys. Rev. Lett. **107**, 052301 (2011), arXiv:1104.1627 [hep-ph] .
- [21] Y. Yin, (2018), arXiv:1811.06519 [nucl-th] .
- [22] P. Romatschke and U. Romatschke, *Relativistic Fluid Dynamics In and Out of Equilibrium*, Cambridge Monographs on Mathematical Physics (Cambridge University Press, 2019) arXiv:1712.05815 [nucl-th] .
- [23] C. Shen and L. Yan, Nucl. Sci. Tech. **31**, 122 (2020), arXiv:2010.12377 [nucl-th] .
- [24] S. K. Singh and J. Alam, (2021), arXiv:2110.15604 [hep-ph] .
- [25] I. Karpenko, P. Huovinen, and M. Bleicher, Computer Physics Communications **185**, 3016 (2014).
- [26] C. Shen and S. Alzhrani, Phys. Rev. C **102**, 014909 (2020).
- [27] P. Parotto, M. Bluhm, D. Mroczek, M. Nahrgang, J. Noronha-Hostler, K. Rajagopal, C. Ratti, T. Schäfer, and M. Stephanov, Phys. Rev. C **101**, 034901 (2020).
- [28] P. Huovinen and H. Petersen, Eur. Phys. J. A **48**, 171 (2012).
- [29] S. S. Gubser, Phys. Rev. D **82**, 085027 (2010).
- [30] P. F. Kolb, J. Sollfrank, and U. W. Heinz, Phys. Rev. C **62**, 054909 (2000), arXiv:hep-ph/0006129 .
- [31] B. Schenke, S. Jeon, and C. Gale, Phys. Rev. C **82**, 014903 (2010), arXiv:1004.1408 [hep-ph] .
- [32] G. S. Denicol, C. Gale, S. Jeon, A. Monnai, B. Schenke, and C. Shen, Phys. Rev. C **98**, 034916 (2018).
- [33] J. R. Cudell, V. V. Ezhela, P. Gauron, K. Kang, Y. V. Kuyanov, S. B. Lugovsky, E. Martynov, B. Niclescu, E. A. Razuvaev, and N. P. Tkachenko (COMPETE Collaboration), Phys. Rev. Lett. **89**, 201801 (2002).
- [34] B. Abelev *et al.* (ALICE Collaboration), Phys. Rev. C **88**, 044909 (2013).
- [35] D. H. Rischke, Y. Pürsün, and J. A. Maruhn, Nuclear Physics A **595**, 383 (1995).
- [36] A. Monnai, S. Mukherjee, and Y. Yin, Phys. Rev. C **95**, 034902 (2017).
- [37] G. S. Denicol, S. Jeon, and C. Gale, Phys. Rev. C **90**, 024912 (2014).
- [38] G. S. Denicol, S. Jeon, and C. Gale, Phys. Rev. C **90**, 024912 (2014).
- [39] M. Stephanov and Y. Yin, Nucl. Phys. A **967**, 876 (2017), arXiv:1704.07396 [nucl-th] .
- [40] M. Stephanov and Y. Yin, Phys. Rev. D **98**, 036006 (2018).
- [41] K. Rajagopal, G. Ridgway, R. Weller, and Y. Yin, Phys. Rev. D **102**, 094025 (2020), arXiv:1908.08539 [hep-ph] .
- [42] H. E. Stanley, Oxford University Press (1971.).